ARTICLE

Diameter-Selective Growth of Single-Walled Carbon Nanotubes with High Quality by Floating Catalyst Method

Qingfeng Liu, Wencai Ren, Zhi-Gang Chen, Da-Wei Wang, Bilu Liu, Bing Yu, Feng Li, Hongtao Cong, and Hui-Ming Cheng*

Shenyang National Laboratory for Materials Science, Institute of Metal Research, Chinese Academy of Sciences, Shenyang 110016, People's Republic of China

ABSTRACT High-quality single-walled carbon nanotubes (SWNTs) with tunable diameters were synthesized by an improved H_2/CH_4-based floating catalyst method. Transmission electron microscopy observations and Raman results demonstrated the overall quality of the as-synthesized samples with finely tailored large diameters at 1.28, 1.62, 1.72, 1.91, and 2.13 nm, depending on the experimental conditions. In addition, Raman analysis revealed that the abundance of specific (*n*, *m*) SWNTs could be selectively enriched simultaneously along with the diameter modulation. It was found that the selective etching effects of high hydrogen flow stabilized the decomposition of ultralow CH_4 flow and considerably suppressed the deposition of amorphous carbon and small nanotubes, leading to very pure samples with high structural homogeneity suitable for further applications in practical electronic systems.

KEYWORDS: carbon nanotubes · diameter · hydrogen · etching · floating catalyst

*Address correspondence to cheng@imr.ac.cn.

Received for review June 3, 2008 and accepted July 25, 2008.

Published online August 7, 2008.
10.1021/nn8003394 CCC: $40.75

Since the pioneering reports of single-walled carbon nanotubes (SWNTs) in 1993,[1,2] they have been widely recognized as potential building blocks in future high-performance nanoelectronics. The characteristics of SWNTs strongly depend on their diameter and chirality denoted by the structural indices (*n*, *m*). For instance, about one-third of SWNTs exhibit metallic properties (M-SWNTs, if $n - m = 3p$, where p is an integer), while the remaining two-thirds act as semiconductor (S-SWNTs, if $n - m = 3p \pm 1$).[3] Moreover, the band gap of S-SWNTs is inversely proportional to tube diameter.[4] However, conventional as-synthesized SWNTs, a mixture of both types of nanotubes, vary sharply in diameter and chirality, which results in striking changes in their electronic properties and optical behaviors.[5,6] Therefore, the currently unavoidable structural heterogeneity of as-synthesized SWNTs substantially prevents their potential applications in practical electronic systems.[7] Accordingly, for the realization of SWNT-based electronics, it is technologically critical to synthesize uniform SWNTs with high quality.

Recently, uniform SWNTs with small diameters (0.6−1.1 nm) have been directly grown on Fe/MgO,[8] Fe/Co,[9] Fe/Mo,[10] Co-MCM-41,[11−13] and Co−Mo[14,15] using various carbon sources such as methane, CO, as well as alcohol by chemical vapor deposition (CVD). However, compared to small nanotubes, large-diameter SWNTs (>1.0 nm) can provide sufficient band gaps for high on/off ratios, enhance mobility, and allow for good electrical contacts[16] and, therefore, are expected to exhibit high performance for nanoelectronics. Postproduction separation methods provide a possible way to obtain uniform SWNTs with small diameters by taking advantage of difference in their physical and chemical properties.[17−21] However, these methods share a common feature that the quality of the resulting SWNTs strongly depends on the starting SWNT materials, besides the resulting SWNTs may be damaged during these harsh treatments. For example, it is not easy to obtain pure S-SWNTs from large-diameter SWNT materials *via* selective etching and gasifying of M-SWNTs by gas-phase plasma.[22] In particular, diameter-based separation is more difficult because differences in physical and chemical properties caused by diameter change are smaller and because variations in tube length can be a dominant factor in physical-based separation methods.[23] Therefore, lager-scale synthesis of large-diameter SWNTs with tunable diameters and (*n*, *m*) enrichment in a narrow distribution is the most urgent and fundamental step toward further separation of SWNTs with desired structure and property for various industrial applications in any field.

Here, we report selective synthesis of large-diameter SWNTs with narrow diameter distribution and high quality by a further improved floating catalyst chemical vapor deposition (FCCVD) technique that is based on our earlier methods of producing large-scale SWNTs.[24,25] The as-synthesized samples have showed a SWNT percentage of more than 95% without any amorphous carbon. Moreover, the diameter of the SWNTs can be finely tailored in the range of 2.1 ± 0.2, 1.9 ± 0.2, 1.7 ± 0.2, 1.6 ± 0.2, and 1.3 ± 0.2 nm, dependent on the experimental conditions. Raman analysis reveals that the abundance of specific (*n*, *m*) SWNTs can also be tuned simultaneously along with the diameter modulation. Such structural homogeneity of the as-synthesized SWNTs has been guaranteed by the selective etching effect of high H_2 flow, which can stabilize the decomposition of ultralow CH_4 flow during the growth reaction.

Figure 1a illustrates a photograph showing the actual size of the as-synthesized SWNT films after a growth time of 30 min. Given that scale up is not limited by the growth process, the synthesis of high-quality SWNTs is easily scaled up by using a larger reaction tube. Figure 1b shows a typical scanning electron microscope (SEM) image of the pristine SWNTs. It can be seen that this sample consists of abundant very clean bundles without any amorphous carbon. Compared to conventional FCCVD-produced SWNTs, the metal particles in the as-synthesized sample are greatly reduced, as observed by transmission electron microscope (TEM, Figure 1c). In our experiments, the growth rate was finely controlled by precisely controlling the sublimation temperature of ferrocene within a 5 °C temperaure range at low temperatures of 60−120 °C, in which ferrocene was very slowly sublimated (Figure S1, Supporting Information), and its subsequent pyrolysis at high temperatures *in situ* produced a limited amount of iron clusters with high activity. High-resolution transmission electron microscopy (HRTEM, the inset in Figure 1c) reveals a perfect hexagonal packing structure in cross section, demonstrating that the bundle consists of uniform SWNTs. These results

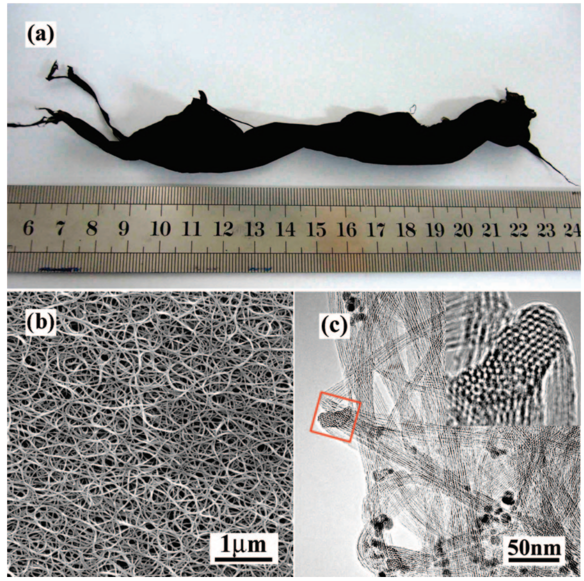

Figure 1. (a) Photograph of the as-synthesized SWNT material after a growth time of 30 min. (b) SEM and (c) TEM images of the pristine SWNTs. Inset in (c) is an enlarged HRTEM image of the framed portion, showing the cross section of a SWNT bundle.

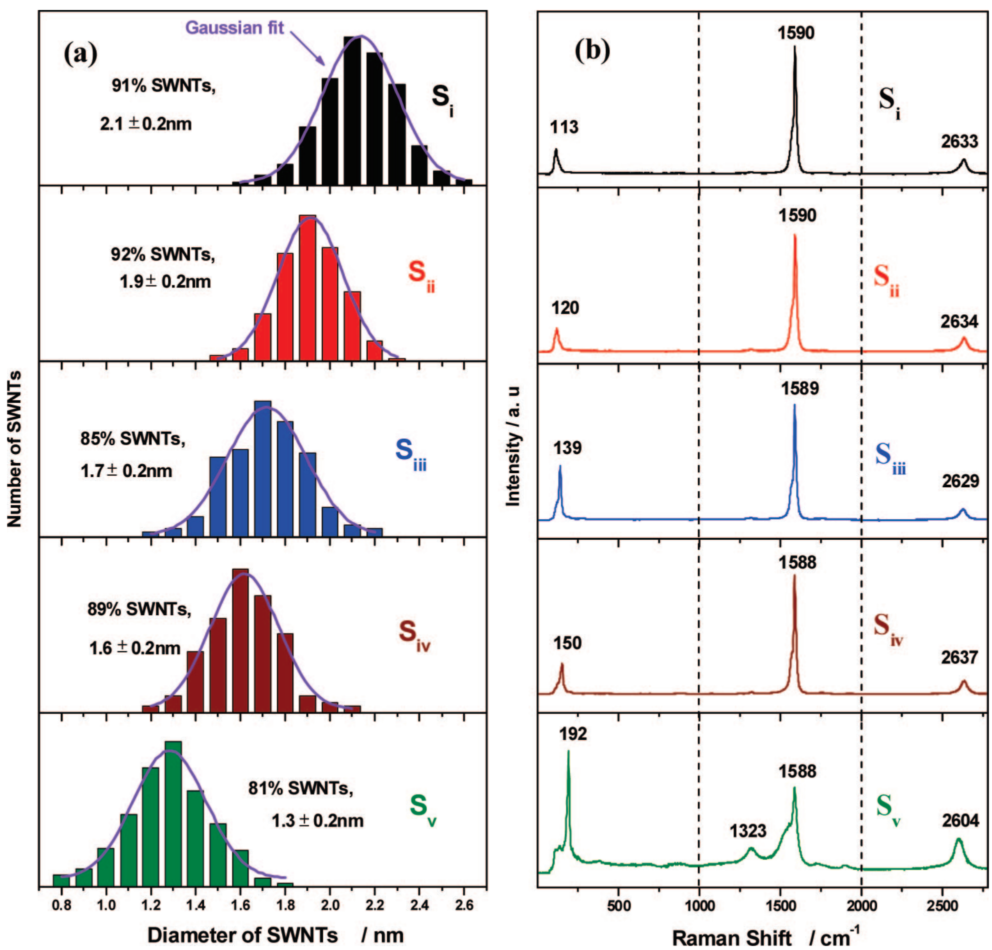

Figure 2. (a) SWNT diameter distributions of sample S_i−S_v and their Gaussian fits with means of 2.13, 1.91, 1.72, 1.62, and 1.28 nm, respectively, measured from a total of 1841 nanotubes from HRTEM images. (b) Raman spectra of sample S_i−S_v, excited by a laser energy of E_{laser} = 1.96 eV.

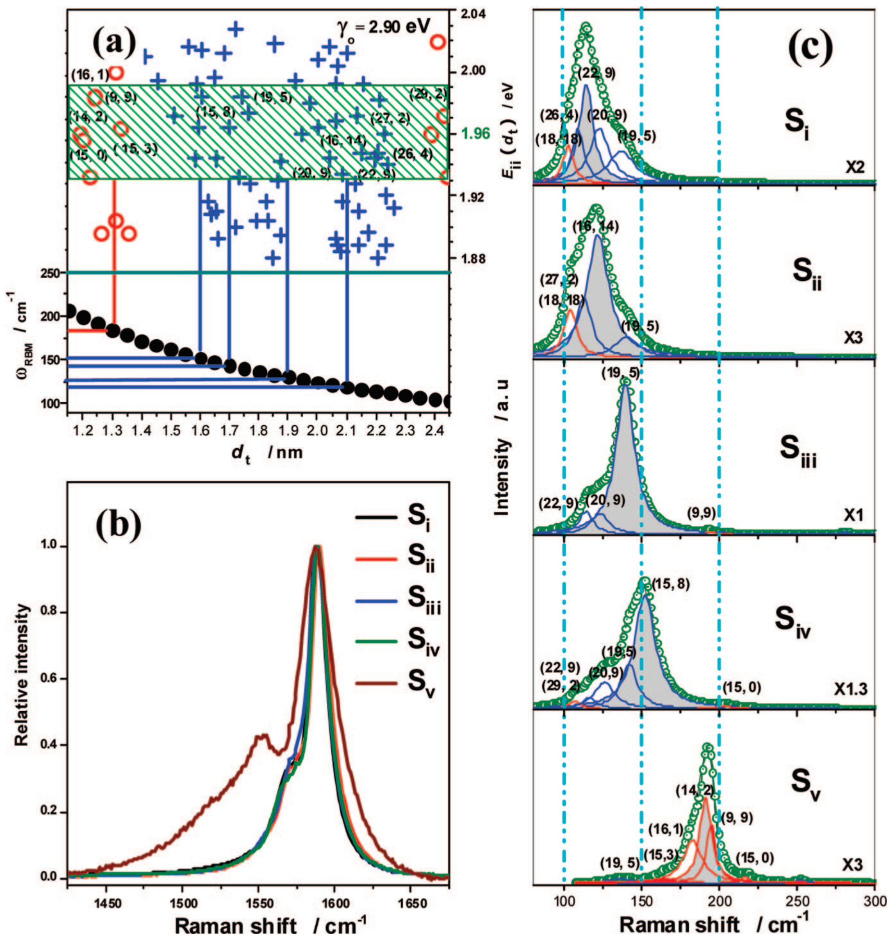

Figure 3. (a) Correlation between E_{ii} (interband energy), ω_{RBM}, and d_t. Horizontal solid line splits the figure into top and bottom panels. Solid circles indicate calculated RBMs from the equation: $\omega_{RBM} = 223.5/d_t + 12.5$. M-SWNTs (open red circles) and S-SWNTs (blue ×'s) are easily distinguishable by their RBMs at excitation wavelenghth λ= 633 nm. (b) Relative intensity of G bands after comparison−normalization for S_i−S_v. (c) Peaks deconvolved from the RBMs. Red and blue lines indicate M-SWNTs and S-SWNTs, respectively.

strongly indicate that the improved H_2/CH_4-based FC-CVD is a promising method for larger-scale production of pure SWNTs with high quality and structural homogeneity.

Depending on the growth conditions (Table S1, Supporting Information), five kinds of samples were obtained and denoted as S_i, S_{ii}, S_{iii}, S_{iv}, and S_v. Figure 2a displays the diameter distribution of SWNTs in each sample, from the analysis of a total of 1841 nanotubes measured from HRTEM images. It can be seen that the diameter of over 80% SWNTs from S_i to S_v is finely tailored in a narrow range of 2.1 ± 0.2, 1.9 ± 0.2, 1.7 ± 0.2, 1.6 ± 0.2, and 1.3 ± 0.2 nm, with the Gaussian mean at 2.13, 1.91, 1.72, 1.62, and 1.28 nm, respectively. It is known that the frequency of radial breathing mode (RBM, ω_{RBM}) of SWNTs is inversely proportional to the tube diameter (d_t): $\omega_{RBM} = 223.5/d_t + 12.5$.[26] Therefore, it can also be estimated from RBMs (Figure 2b) that the SWNTs from S_i to S_v have average diameters of 2.24, 2.04, 1.77, 1.61, and 1.25 nm, respectively, well in agreement with the above statistical analysis. Moreover, there is only one narrow peak in the RBM regions, and it shifts from low to high frequency from S_i to S_v, further demonstrating that the structure of SWNTs is exceptionally homogeneous and tunable. The D band in graphite involves scattering from a defect which breaks the basic symmetry of the graphene sheet, and it can be observed in SWNTs containing vacancies, impurities, or other symmetry-breaking defects.[27] In Figure 2b, the D band is almost absent for S_i−S_{iv}, indicating high quality of the SWNTs, which is consistent with the above SEM and TEM observations.

According to the Kataura plot (the upper panel of Figure 3a),[28] giving the resonant van Hove singularity in the joint density of states for all (n, m) SWNTs as a function of tube diameter ($d_t = 0.249(n^2 + m^2 + mn)^{1/2}/\pi$),[27] we can obtain information about the abundance of M/S-SWNTs in each sample. It is apparent that the enrichment of metallic tubes in S_v is dramatically increased, compared to other samples. If there were some M-SWNTs with diameters in the range of 1.2−1.5 nm (the lower panel of Figure 3a) for S_{iii} and S_{iv}, corresponding RBM peaks would rather be expected than be suppressed. This allows us to conclude that all nanotubes with a diameter in the range of 1.2−1.5 nm are semiconducting for S_{iii} and S_{iv}. Additionally, comparison of the G band regions further supports this argument.[29] Typically, both M-SWNTs and S-SWNTs can characteristically show two dominant features between 1500 and 1600 cm^{-1} at room temperature, the lower frequency component (ω_{G-}) associated with vibrations along the circumferential direction, and the higher frequency component (ω_{G+}) attributed to vibrations along the direction of the nanotube axis. Both ω_{G-} and ω_{G+} in S-SWNTs show a narrow and symmetric Lorentzian line shape, while ω_{G+} in M-SWNTs has a Lorentzian line shape that is almost as narrow as that for S-SWNTs, but ω_{G-} is a very broad and asymmetric Breit−Wigner−Fano (BWF) line.[27] Therefore, the much broader ω_{G-} component (centered at ~1540 cm^{-1}) of S_v (Figure 3b) not only provides additional confirmation that this sample is enriched with metallic tubes but also reflects the smaller diameter in S_v. Furthermore, the resistivities of S_i to S_v were measured by using four-point probe technique. The electric conductivity of the bulky film from S_v (~6.2

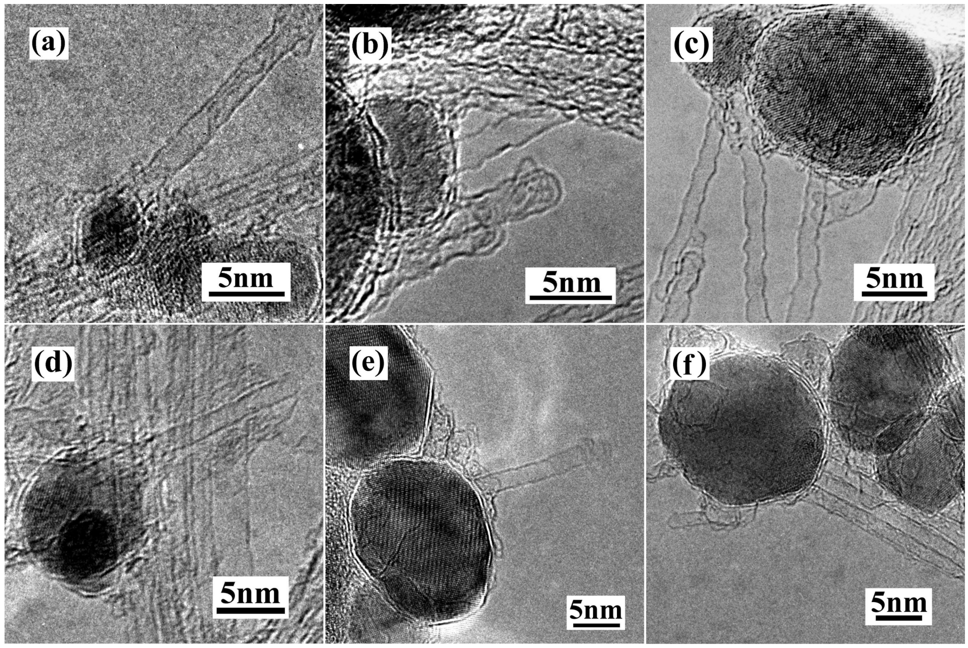

Figure 4. HRTEM images for FCCVD-based SWNTs grown from catalyst particles.

m$\Omega \cdot$cm) is 1.6−11 times higher than those of S_i−S_{iv}, which qualitatively indicates the existence of more metallic nanotubes, in agreement with the Raman data.

Additionally, according to the Kataura plot, there are many different (*n*, *m*) SWNT species within the resonance window (1.86−2.06 eV) for the laser excitation energy of 1.96 eV, for a SWNT product with the same diameter distribution as S_i to S_v. However, only several peaks (Figure 3c) are deconvolved from the RBM features. Considering the very narrow line width of each deconvolved peak, we believe that the number of (*n*, *m*) species should be much smaller than those theoretically predicted, meaning that there is a (*n*, *m*) selectivity of SWNTs in these samples. Note that some deconvolved RBM peaks have similar frequencies for S_i to S_v, such as 103, 112, 114, 122, 140, and 193 cm^{-1}. This makes it possible to identify the (*n*, *m*) selectivity of these samples from RBM analysis. Here, the relative quantities of (*n*, *m*) SWNTs for each sample are evaluated by the relative integrated intensities of the Lorentzians, which allows us to eliminate the unknown resonance enhancement factors for the individual (*n, m*) SWNTs contributing to the spectra, thus avoiding a specific (*n*, *m*) assignment. Table S2 in the Supporting Information lists the integrated intensities of all Lorentzians that fit the RBM features. It is clear that the relative intensity of 114, 122, 140, 151, and 193 cm^{-1} is largest for S_i, S_{ii}, S_{iii}, S_{iv}, and S_v, respectively. Each RBM peak of a SWNT ensemble could be considered as a superposition of several narrower Raman lines corresponding to the tubes with nearly same diameters.[30] However, according to the calculated diameter and the Kataura plot, the RBM peaks in Figure 3c can be tentatively assigned to five groups of (*n*, *m*) tubes: (18, 18)/(26, 4)/(22, 9)/(20, 9)/(19, 5), (18, 18)/(27, 2)/(16, 14)/(19, 5), (22, 9)/(20, 9)/(19, 5), (29, 2)/(22, 9)/(20, 9)/ (19, 5) /(15, 8), and (16, 1)/(14, 2)/(9, 9)/(15, 0), respectively. This result suggests that the abundance of (*n*, *m*) SWNTs can be also tuned simultaneously with diameter by adjusting experimental parameters.

In our experiments, ultralow carbon feeding rate (<~6 sccm) and high hydrogen flow rate (1500−3000 sccm) are two key factors to obtain uniform SWNTs. Once the rate of CH_4 flow is over 10 sccm, the as-synthesized SWNTs typically have a broad diameter distribution, which can be seen from their Raman spectra (Figure S2, Supporting Information). Meanwhile, when pure Ar flow is used as carrier gas, the diameter distribution of the SWNTs remarkably increases (Figure S3, Supporting Information). Generally, with the above two prerequisites, larger SWNTs are closely related to higher flow rates of carrier gas, lower sublimation temperatures of ferrocene, lower carbon feeding rates, and lower growth temperatures. It should be noted that the microstructure of SWNTs is independent of the reaction duration time because FCCVD is a continuous process, in which SWNTs are grown and quickly transported out of the reaction zone by carrier gas.

It is well accepted that kinetic rather than thermodynamic should be considered to explain the population of a given nanotube sample.[14,15,31] For instance, when coordinated to the metal surface, the nanotube cap for an armchair nanotube (a regular array of atoms) tends to be most stable, and thus the growth of the armchair nanotube has the lowest (kinetic) activation energy.[32] Clearly, the activation energy for SWNT growth varies from one type to another. It is conceivable that variations of experimental conditions will result in different kinetic behaviors and consequently lead to the diameter and (*n*, *m*) selectivity of SWNTs. Hydrogen, which is also a byproduct of CH_4 decomposition, can suppress the CH_4 decomposition on the metal cluster surface. So the molar ratio of H_2, CH_4, and ferrocene in the reactor will influence the decomposition rate of CH_4 on the iron cluster surface and thus determine the formation of the nanotube cap with a certain structure, even when the growth temperature is kept constant.

When compared to the previously reported small SWNTs (0.6−1.1 nm),[11,14,15] the growth of large-

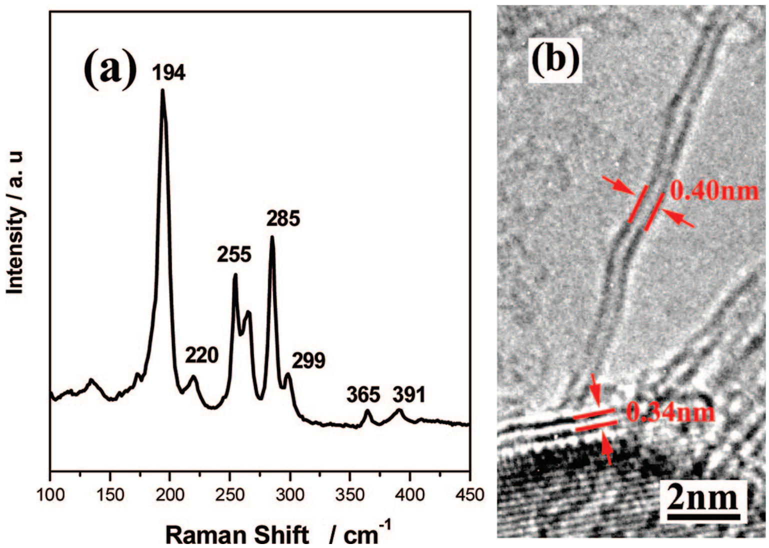

Figure 5. (a) Low-frequency RBM of the SWNTs. (b) Smallest freestanding 0.4 nm diameter nanotube obtained by Ar/CH_4-based FCCVD.

diameter SWNTs in H_2/CH_4-based FCCVD synthesis can be linked to the evolution of hydrogen, which has a dual effect on the nucleation of carbon and formation of nanotube cap. First, H_2 can increase the rate of reduction (decomposing inactive surface carbides into catalytically active metallic form and gasifying residual surface carbon radicals to maintain a clean surface),[33] sinter metal clusters, and finally cause a broad distribution of metal particles. This result contrasts with the narrow size range obtained with pure Ar as carrier gas (Figure S4, Supporting Information). With CH_4 as carbon feedstock, the size of metal clusters is not only determined by H_2 but also by the extent of CH_4 conversion, which in turn varies the metal cluster exposure to H_2. Second, H_2 can also lower the carbon surface fugacity on the metal cluster surface, a well-known phenomenon in heterogeneous catalysis.[34] The decrease of carbon fugacity on the metal cluster surface will delay the nucleation of the cap. If during this delay the metal cluster continues growing by metal sintering, the formation of the cap will occur at a larger diameter.[32]

The narrow distribution in diameter and the enrichment of M/S-SWNTs deserve some discussion. In the literature, many researchers believe that the uniformity of SWNT diameter results most likely from the uniformity of catalyst particles with similar size to SWNT diameter.[8−11] However, on the basis of a great deal of HRTEM observations, we found that the final size of catalyst particles varies greatly, larger than the diameter of SWNTs grown from them, as shown in Figure 4a−f. Clearly, these findings have painted a more complex picture than the simple idea that the SWNT diameter is determined by the size of catalyst particles. For example, Yao *et al.*[35] also found that the diameter of a SWNT could vary with growth temperature even though the catalyst particle at the growing tip remains the same. As mentioned above, two prerequisites for the synthesis of uniform SWNTs in our experiments are ultralow carbon feeding rate and high hydrogen flow rate. As far as the dependence of the SWNT diameter on carbon feeding rate is concerned, Lu *et al.*[36] believed that the diameter of SWNTs was closely related to the concentration of carbon atoms (or carbon feeding rate) *via* selective activation of catalyst nanoparticles; here we will not discuss it in detail but focus our attention on the role of hydrogen, which exerts a determinant influence upon the structural homogeneity of the as-synthesized SWNTs. It is worthy noting that, in previous publications,[37,38] hydrogen is notoriously unfavorable to SWNT formation and growth, likely due to attacking of the sp^2 C to form sp^3 structures,[39,40] giving a low-yield growth of SWNTs. For example, Zhang *et al.*[37] pointed out that even 10% H_2 would substantially yield a blocking effect of reactive H radicals on SWNT growth in CH_4-based plasma-enhanced chemical vapor deposition (PECVD) even at room temperature. In our experiments, however, uniform SWNTs can be synthesized only with high hydrogen flow ($H_2 = \sim$99.7%), strongly indicating that H_2 has a positive effect on the structural uniformity of SWNTs in H_2/CH_4-based FCCVD synthesis.

In fact, when compared to the PECVD case, the concentration of reactive H radicals in thermal CVD is about 10^6 times lower,[41] which may not considerably change the surface kinetics or block the formation of sp^2-like SWNTs; nevertheless, the moderate etching effects of these atomic hydrogens on SWNTs should be expected at high temperatures *via* the following reactions:

$$\text{(i-SWNTs + r-SWNTs)} + \text{H} \rightarrow \text{(i-SWNTs)} + CH_x, C_2H_y, C_3H_z \ldots$$

$$CH_x, CH_y, C_3H_z \ldots + \text{H} \rightarrow CH_4\uparrow, C_2H_6\uparrow, C_3H_8\uparrow \ldots$$

where i-SWNTs and r-SWNTs are relatively chemically inert and reactive SWNTs, respectively, and x, y, and z are integers. Especially, such selective etching of low concentration of reactive H radicals is more pronounced for small-diameter or metallic nanotubes since both types are more reactive to be attacked preferentially.[40,42] This hypothesis is consistent with our results that large SWNTs (>1.0 nm) were synthesized by H_2/CH_4-based FCCVD, with few tubes with a diameter <0.7 nm. In stark contrast, Ar/CH_4-based FCCVD synthesis produces abundant small SWNTs with a diameter <0.7 nm, which can be seen from their Raman spectra (Figure 5a). Interestingly, even the smallest freestanding tubes with diameter of 0.40 nm can be frequently found during HRTEM observations, as shown in Figure 5b. Meanwhile, lower growth temperature will decrease the etching effects and the amount of reactive H radicals; therefore, smaller M-SWNTs largely assemble in sample S_v. On the contrary, higher growth temperature leads to the enrichment of larger S-SWNTs in samples of S_i to S_{iv}. This process is very similar to the separation progressing of S-SWNTs *via* selectively etching and gasifying M-SWNTs by gas plasma.[22] Therefore, we believe that the selective etching effects of low concentration of reactive H radicals are responsible for the structural homogeneity of the SWNTs in H_2/CH_4-based FCCVD synthesis. Second, the deposition of amorphous carbon on SWNTs can also be easily gasified and removed by the etching effects of reactive H radicals *via* the following reactions:

$$(\text{SWNT})\text{-CH}_n + \text{H} \rightarrow (\text{SWNT})\text{-CH}_{n+1}\ (n = 0, 1, 2)$$

$$(\text{SWNT})\text{-CH}_3 + \text{H} \rightarrow (\text{SWNT}) + \text{CH}_4\uparrow$$

and thus high-quality SWNTs are obtained without amorphous carbon on tube surface, which is well in agreement with the above results of SEM, TEM, and Raman. Finally, CH_4 dissociation process can be enabled by atomic hydrogen due to the abstraction reaction ($CH_4 + H \rightarrow CH_3 + H_2$),[43] thereby facilitating carbon deposition and diffusion on the surface of metal catalyst. It should be noted that, once hydrogen flow is used as only carrier gas with a rate of >3000 or <200 sccm, this method gives a poor yield of SWNTs because the etching effects are enhanced in both extreme cases, excessively gasifying surface carbon (before solvation) or even preventing dissociative adsorption by blocking active sites.[33] The former is attributed to the increasing concentration of reactive H radicals, besides the nanotube growth time is simultaneously shortened; the latter may be due to the increase of etching time because SWNTs are transported more slowly out of the reaction zone at a lower flow rate.

In summary, we have demonstrated that high-quality SWNTs with tunable diameter distribution and (*n*, *m*) enrichment can be synthesized by H_2/CH_4-based FCCVD method. The diameter and (*n*, *m*) selectivity of SWNTs are attributed to the selective etching effects of low concentration of reactive H radicals, which provides a remarkable tool for tailoring specific carbon nanotubes even without the need of postgrowth separation methods and thus opens up a possibility for large-scale SWNT electronics with high performance.

METHODS

The synthesis was performed in a quartz tube reactor inside an electrical furnace. In a typical experiment, 100−4000 sccm H_2 (or H_2/Ar) flow was introduced through the quartz tube. When the reaction temperature reached 900−1200 °C, a mixture of ferrocene/sulfur powder (S = 0.5 wt %) was sublimated at 50−120 °C and transported into the reaction zone by the gas flow. At the same time, no more than ~6 sccm CH_4 flow was introduced, and then SWNTs grew downstream inside the quartz tube. After a growth time of 10−60 min, the furnace was cooled naturally to room temperature under the protection of H_2. It is worth noting that, when compared to our earlier preparation procedure,[24,25] some improvements were made to obtain uniform SWNTs, including the following: (i) high H_2 flow and ultralow CH_4 flow were used to stabilize the decomposition of ultralow CH_4 flow in order to realize a better structural control; (ii) to avoid the influence of heat inertia of the furnace that could induce an additional sublimation of ferrocene and thus increase the amount of iron particles in the as-synthesized SWNT samples, ferrocene was removed quickly to the sublimation zone from the cold zone (near to room temperature) when the growth reaction started, and then removed to the cold zone after the growth reaction; (iii) the sublimation rate of ferrocene was finely restricted by controlling its sublimation temperature within a 5 °C temperaure range; and (iv) sulfur powder was used as growth promoter instead of thiophene, and then a precise ratio of catalyst/promoter can be maintained during the growth reaction.

Acknowledgment. The authors acknowledge financial support from the Ministry of Science and Technology of China (No. 2006CB932701 and No. 2008DFA51400), National Science Foundation of China (No. 90606008 and No. 50702063), and Chinese Academy of Sciences (No. KJCX2-YW-M01).

Supporting Information Available: Thermogravimetric analysis of ferrocene with 10 °C/min heating rate; growth conditions for S_i−S_v; integrated intensities of all Lorentzians that fit the RBM features for S_i−S_v; Raman spectra of the as-synthesized SWNTs by H_2/CH_4-based FCCVD; diameter distributions of the as-synthesized SWNTs by Ar/CH_4-based FCCVD; diameter distributions of the Fe-NPs in H_2 (Ar)/CH_4-based FCCVD synthesis. This material is available free of charge *via* the Internet at http://pubs.acs.org.

REFERENCES AND NOTES

1. Iijima, S.; Ichihashi, T. Single-Shell Carbon Nanotubes of 1-nm Diameter. *Nature* **1993**, *363*, 603–605.
2. Bethune, D. S.; Kiang, C. H.; Devries, M. S.; Gorman, G.; Savoy, R.; Vazquez, J.; Beyers, R. Cobalt-Catalyzed Growth of Carbon Nanotubes with Single-Atomic-Layerwalls. *Nature* **1993**, *363*, 605–607.
3. Dresselhaus, M. S. Nanotubes—A Step in Synthesis. *Nat. Mater.* **2004**, *3*, 665–666.
4. Odom, T. W.; Huang, J. L.; Kim, P.; Lieber, C. M. Atomic Structure and Electronic Properties of Single-Walled Carbon Nanotubes. *Nature* **1998**, *391*, 62–64.
5. Arnold, M. S.; Green, A. A.; Hulvat, J. F.; Stupp, S. I.; Hersam, M. C. Sorting Carbon Nanotubes by Electronic Structure Using Density Differentiation. *Nat. Nanotechnol.* **2006**, *1*, 60–65.
6. Konduri, S.; Mukherjee, S.; Nair, S. Controlling Nanotube Dimensions: Correlation between Composition, Diameter, and Internal Energy of Single-Walled Mixed Oxide Nanotubes. *ACS Nano* **2007**, *1*, 393–402.
7. Baughman, R. H.; Zakhidov, A. A.; de Heer, W. A. Carbon Nanotubes—The Route toward Applications. *Science* **2002**, *297*, 787–792.
8. Ago, H.; Imamura, S.; Okazaki, T.; Saitoj, T.; Yumura, M.; Tsuji, M. CVD Growth of Single-Walled Carbon Nanotubes with Narrow Diameter Distribution over Fe/MgO Catalyst and Their Fluorescence Spectroscopy. *J. Phys. Chem. B* **2005**, *109*, 10035–10041.
9. Inoue, S.; Kikuchi, Y. Diameter Control and Growth Mechanism of Single-Walled Carbon Nanotubes. *Chem. Phys. Lett.* **2005**, *410*, 209–212.
10. An, L.; Owens, J. M.; McNeil, L. E.; Liu, J. Synthesis of Nearly Uniform Single-Walled Carbon Nanotubes Using Identical Metal-Containing Molecular Nanoclusters as Catalysts. *J. Am. Chem. Soc.* **2002**, *124*, 13688–13689.

11. Ciuparu, D.; Chen, Y.; Lim, S.; Haller, G. L.; Pfefferle, L. Uniform-Diameter Single-Walled Carbon Nanotubes Catalytically Grown in Cobalt-Incorporated MCM-41. *J. Phys. Chem. B* **2004**, *108*, 503–507.
12. Chen, Y.; Ciuparu, D.; Lim, S.; Yang, Y. H.; Haller, G. L.; Pfefferle, L. Synthesis of Uniform Diameter Single Wall Carbon Nanotubes in Co-MCM-41: Effects of Co Pressure and Reaction Time. *J. Catal.* **2004**, *226*, 351–362.
13. Chen, Y.; Wei, L.; Wang, B.; Lim, S. Y.; Ciuparu, D.; Zheng, M.; Chen, J.; Zoican, C.; Yang, Y. H.; Haller, G. L. Low-Defect, Purified, Narrowly (*n*,*m*)-Dispersed Single-Walled Carbon Nanotubes Grown from Cobalt-Incorporated MCM-41. *ACS Nano* **2007**, *1*, 327–336.
14. Wang, B.; Poa, C. H. P.; Wei, L.; Li, L. J.; Yang, Y. H.; Chen, Y. (*n*,*m*) Selectivity of Single-Walled Carbon Nanotubes by Different Carbon Precursors on Co-Mo Catalysts. *J. Am. Chem. Soc.* **2007**, *129*, 9014–9019.
15. Bachilo, S. M.; Balzano, L.; Herrera, J. E.; Pompeo, F.; Resasco, D. E.; Weisman, R. B. Narrow (*n*,*m*)-Distribution of Single-Walled Carbon Nanotubes Grown Using a Solid Supported Catalyst. *J. Am. Chem. Soc.* **2003**, *125*, 11186–11187.
16. Kim, W.; Javey, A.; Tu, R.; Cao, J.; Wang, Q.; Dai, H. J. Electrical Contacts to Carbon Nanotubes Down to 1 nm in Diameter. *Appl. Phys. Lett.* **2005**, *87*, 173101.
17. Campidelli, S.; Meneghetti, M.; Prato, M. Separation of Metallic and Semiconducting Single-Walled Carbon Nanotubes *via* Covalent Functionatization. *Small* **2007**, *3*, 1672–1676.
18. Chattopadhyay, D.; Galeska, L.; Papadimitrakopoulos, F. A Route for Bulk Separation of Semiconducting from Metallic Single-Wall Carbon Nanotubes. *J. Am. Chem. Soc.* **2003**, *125*, 3370–3375.
19. Strano, M. S.; Dyke, C. A.; Usrey, M. L.; Barone, P. W.; Allen, M. J.; Shan, H. W.; Kittrell, C.; Hauge, R. H.; Tour, J. M.; Smalley, R. E. Electronic Structure Control of Single-Walled Carbon Nanotube Functionalization. *Science* **2003**, *301*, 1519–1522.
20. Krupke, R.; Hennrich, F.; von Lohneysen, H.; Kappes, M. M. Separation of Metallic from Semiconducting Single-Walled Carbon Nanotubes. *Science* **2003**, *301*, 344–347.
21. Arnold, M. S.; Stupp, S. I.; Hersam, M. C. Enrichment of Single-Walled Carbon Nanotubes by Diameter in Density Gradients. *Nano Lett.* **2005**, *5*, 713–718.
22. Zhang, G. Y.; Qi, P. F.; Wang, X. R.; Lu, Y. R.; Li, X. L.; Tu, R.; Bangsaruntip, S.; Mann, D.; Zhang, L.; Dai, H. J. Selective Etching of Metallic Carbon Nanotubes by Gas-Phase Reaction. *Science* **2006**, *314*, 974–977.
23. Zheng, M.; Jagota, A.; Strano, M. S.; Santos, A. P.; Barone, P.; Chou, S. G.; Diner, B. A.; Dresselhaus, M. S.; McLean, R. S.; Onoa, G. B.; et al. Structure-Based Carbon Nanotube Sorting by Sequence-Dependent DNA Assembly. *Science* **2003**, *302*, 1545–1548.
24. Cheng, H. M.; Li, F.; Su, G.; Pan, H. Y.; He, L. L.; Sun, X.; Dresselhaus, M. S. Large-Scale and Low-Cost Synthesis of Single-Walled Carbon Nanotubes by the Catalytic Pyrolysis of Hydrocarbons. *Appl. Phys. Lett.* **1998**, *72*, 3282–3284.
25. Cheng, H. M.; Li, F.; Sun, X.; Brown, S. D. M.; Pimenta, M. A.; Marucci, A.; Dresselhaus, G.; Dresselhaus, M. S. Bulk Morphology and Diameter Distribution of Single-Walled Carbon Nanotubes Synthesized by Catalytic Decomposition of Hydrocarbons. *Chem. Phys. Lett.* **1998**, *289*, 602–610.
26. Bachilo, S. M.; Strano, M. S.; Kittrell, C.; Hauge, R. H.; Smalley, R. E.; Weisman, R. B. Structure-Assigned Optical Spectra of Single-Walled Carbon Nanotubes. *Science* **2002**, *298*, 2361–2366.
27. Dresselhaus, M. S.; Dresselhaus, G.; Jorio, A.; Souza, A. G.; Saito, R. Raman Spectroscopy on Isolated Single Wall Carbon Nanotubes. *Carbon* **2002**, *40*, 2043–2061.
28. Kataura, H.; Kumazawa, Y.; Maniwa, Y.; Umezu, I.; Suzuki, S.; Ohtsuka, Y.; Achiba, Y. Optical Properties of Single-Wall Carbon Nanotubes. *Synth. Met.* **1999**, *103*, 2555–2558.
29. Wang, Y.; Liu, Y. Q.; Li, X. L.; Cao, L. C.; Wei, D. C.; Zhang, H. L.; Shi, D. C.; Yu, G.; Kajiura, H.; Li, Y. M. Direct Enrichment of Metallic Single-Walled Carbon Nanotubes Induced by the Different Molecular Composition of Monohydroxy Alcohol Homologues. *Small* **2007**, *3*, 1486–1490.
30. Iliev, M. N.; Litvinchuk, A. P.; Arepalli, S.; Nikolaev, P.; Scott, C. D. Fine Structure of the Low-Frequency Raman Phonon Bands of Single-Wall Carbon Nanotubes. *Chem. Phys. Lett.* **2000**, *316*, 217–221.
31. Maiti, A.; Brabec, C. J.; Bernholc, J. Kinetics of Metal-Catalyzed Growth of Single-Walled Carbon Nanotubes. *Phys. Rev. B* **1997**, *55*, R6097–R6100.
32. Lolli, G.; Zhang, L. A.; Balzano, L.; Sakulchaicharoen, N.; Tan, Y. Q.; Resasco, D. E. Tailoring (*n*,*m*) Structure of Single-Walled Carbon Nanotubes by Modifying Reaction Conditions and the Nature of the Support of Como Catalysts. *J. Phys. Chem. B* **2006**, *110*, 2108–2115.
33. Vander Wal, R. L.; Hall, L. J. Ferrocene as a Precursor Reagent for Metal-Catalyzed Carbon Nanotubes: Competing Effects. *Combust. Flame* **2002**, *130*, 27–36.
34. Iglesia, E.; Baumgartner, J. E.; Price, G. L. Kinetic Coupling and Hydrogen Surface Fugacities in Heterogeneous Catalysis 0.1. Alkane Reactions on Te/Nax, H-Zsm5, and Ga/H-Zsm5. *J. Catal.* **1992**, *134*, 549–571.
35. Yao, Y. G.; Li, Q. W.; Zhang, J.; Liu, R.; Jiao, L. Y.; Zhu, Y. T.; Liu, Z. F. Temperature-Mediated Growth of Single-Walled Carbon-Nanotube Intramolecular Junctions. *Nat. Mater.* **2007**, *6*, 283–286.
36. Lu, C. G.; Liu, J. Controlling the Diameter of Carbon Nanotubes in Chemical Vapor Deposition Method by Carbon Feeding. *J. Phys. Chem. B* **2006**, *110*, 20254–20257.
37. Zhang, G. Y.; Mann, D.; Zhang, L.; Javey, A.; Li, Y. M.; Yenilmez, E.; Wang, Q.; McVittie, J. P.; Nishi, Y.; Gibbons, J.; et al. Ultra-High-Yield Growth of Vertical Single-Walled Carbon Nanotubes: Hidden Roles of Hydrogen and Oxygen. *Proc. Natl. Acad. Sci. U.S.A.* **2005**, *102*, 16141–16145.
38. Okita, A.; Suda, Y.; Oda, A.; Nakamura, J.; Ozeki, A.; Bhattacharyya, K.; Sugawara, H.; Sakai, Y. Effects of Hydrogen on Carbon Nanotube Formation in CH_4/H-2 Plasmas. *Carbon* **2007**, *45*, 1518–1526.
39. Nikitin, A.; Ogasawara, H.; Mann, D.; Denecke, R.; Zhang, Z.; Dai, H.; Cho, K.; Nilsson, A. Hydrogenation of Single-Walled Carbon Nanotubes. *Phys. Rev. Lett.* **2005**, *95*, 225507.
40. Park, S.; Srivastava, D.; Cho, K. Generalized Chemical Reactivity of Curved Surfaces: Carbon Nanotubes. *Nano Lett.* **2003**, *3*, 1273–1277.
41. Hash, D. B.; Meyyappan, M. Model Based Comparison of Thermal and Plasma Chemical Vapor Deposition of Carbon Nanotubes. *J. Appl. Phys.* **2003**, *93*, 750–752.
42. Lu, J.; Lai, L.; Luo, G.; Zhou, J.; Qin, R.; Wang, D.; Wang, L.; Mei, W. N.; Li, G.; Gao, Z.; et al. Why Semiconducting Single-Walled Carbon Nanotubes Are Separated from Their Metaltic Counterparts. *Small* **2007**, *3*, 1566–1576.
43. Meyyappan, M.; Delzeit, L.; Cassell, A.; Hash, D. Carbon Nanotube Growth by PECVD: A Review. *Plasma Sources Sci. Technol.* **2003**, *12*, 205–216.